Papers submitted to the Conference "Applications of Physics in Mechanical and Material Engineering"

Microstructure and High Temperature Oxidation of Modified Ductile Ni-Resist Alloy with Higher Manganese Content

M.M. Rashidi[a,*], M.H. Idris[b], Z. Shayfull[c], A.H. Ahmad[a], M.M.A. Abdullah[d], P. Pietrusiewicz[e], M. Nabiałek[e] and J. Garus[f]

[a] *Faculty of Mechanical and Automotive Engineering Technology, Universiti Malaysia Pahang, 26600 Pekan, Pahang, Malaysia*
[b] *Department of Materials Engineering, Faculty of Mechanical Engineering, Universiti Teknologi Malaysia, 81310 Skudai, Johor, Malaysia*
[c] *Faculty of Mechanical Engineering Technology, Universiti Malaysia Perlis, Kampus Tetap Pauh Putra, 02600 Arau, Perlis, Malaysia*
[d] *Faculty of Chemical Engineering Technology, Universiti Malaysia Perlis, Kampus Tetap Pauh Putra, 02600 Arau, Perlis, Malaysia*
[e] *Department of Physics, Faculty of Production Engineering and Materials Technology, Czestochowa University of Technology, al. Armii Krajowej 19, 42-200 Częstochowa, Poland*
[f] *Department of Mechanics and Fundamentals of Machinery Design,Faculty of Mechanical Engineering and Computer Science, Częstochowa University of Technology, Dąbrowskiego 73, 42-201 Częstochowa, Poland*

Doi: 10.12693/APhysPolA.142.56 *e-mail: mrashidi@ump.edu.my

In this study, ductile Ni-resist with a minimum of 18 wt% nickel composition was modified. Up to 12 wt% manganese was added together with 10 wt% nickel to investigate the effects of the alloying elements on its microstructure, mechanical properties and isothermal oxidation behaviour. The results show a higher manganese composition on modified ductile Ni-resist with increased carbide formation, and a slightly decreased elevated temperature tensile strength. The addition of higher Mn [wt%] slightly increased the oxidation resistance. Three different oxide layers were observed on the modified ductile Ni-resist after 25 h hot corrosion at 765°C.

topics: Ni-resist alloy, manganese, high temperature oxidation, modified ductile

1. Introduction

Ductile nickel-resist (DNR) with an austenite structure is a material developed for high temperature applications due to a combination with austenitic matrix, which occurs at all temperatures. For comparison, in applications at high temperature of up to 675°C, cast iron and steel pass through a critical range that frequently results in the cracking and distortion of castings [1]. This phenomenon happens due to volume changes, which occur because of matrix phase changes between ferrite and austenite. DNR alloys, as an austenitic matrix at all temperatures, do not undergo this transformation and contribute to a high temperature application [2]. A recent study has reported that nickel (Ni) was accepted as the prime alloying element for processing DNR. The as-cast austenite microstructure of DNR occurs due to the influence of Ni contained in the metal composition, which acts as an austenite matrix stabilizer. Ni suppresses austenite (γ) $\rightarrow$ ferrite (α) changes into conventional ductile iron at a minimum of 18 wt% [3]. They also reported the potential of manganese (Mn) and copper as an alternative to the DNR alloying element. However, those results have shown a dissimilar effect. This study attempted to combine both Ni and Mn at a certain composition in order to produce a DNR alloy. Ni [wt%] was reduced to as low as 10 wt%, and Mn [wt%] was increased to as high as 12 wt%. This modified alloy should form an austenite structure with a graphite nodule in its microstructure. The research will simulate environmental conditions that are suitable for elevated applications at up to 765°C, such as furnace parts, exhaust lines, and valve guides.

TABLE I

Chemical composition of iron, alloyed materials, nodularizer, inoculant, FeMn, and FeCr [wt%].

	Element										
	C	Si	Mn	P	S	Mg	Ni	Ca	Cr	RE	Fe
pig iron	2.91	2.28	0.12	0.07	0.02	–	0.02	–	–	–	balance
steel	2.91	2.28	0.12	0.07	0.02	–	0.02	–	–	–	balance
nickel	–	–	–	–	–	–	99.00	–	–	–	balance
FeMn	–	1.00	86.00	0.10	0.02	–	–	–	–	–	–
FeCr	8.00	4.00	–	0.04	0.04	–	–	–	60.00	–	–
nodularizer	–	44.00	–	–	–	5.00	–	2.00	–	1.90	–
inoculant	–	77.00	–	–	–	–	2.00	–	–	–	balance

2. Experimental procedures

The charge materials (steel scrap, pig iron and pure nickel) used to produce modified DNR with targeted composition were as follows: (i) 9Mn–10Ni, (ii) 10Mn–10Ni, (iii) 11Mn–10Ni, and (iv) 12Mn–10Ni wt%. After sessions of stirring in an induction furnace, ferro–manganese (FeMn) and ferro–chrome (FeCr) were added to increase manganese and chromium content, as shown in Table I. The melt was initially superheated to 1500 ± 20°C and treated for cleanness before being poured at 1400 ± 20°C into a mould. The mould was made with a mixture of silica sand, bentonite, and water to produce a green sand mould. Magnesium treatment and inoculation were performed using the in-mould method. A nodularizer was added to 1.1 wt% in the mould reaction chamber using FeSiMg with a magnesium content of 5% and a size of about 1–4 mm. The runner system for each casting contains a suitably designed chamber in which both nodulant and inoculant were placed. An inoculant with a size ranging from 0.2 to 0.7 mm was employed to encourage the inoculant to dissolve. Test specimens were obtained from ASTM A439 Y-blocks. Metallographic samples were sectioned, grounded and polished with 0.3 μm alumina powder. Table I lists all kinds of experimental chemical compositions used. After the specimen was sectioned, the samples were exposed for 25 h at 765°C in furnace atmosphere–air, where the temperature increased at a rate of 70°C/min. After exposure, the specimen was checked under Jeol JSM-6380LA Scanning Electron Microscope (SEM), which was used to determine elemental and microstructure analysis. X-ray diffractometer (XRD) with Cu $K_{\alpha 1}$ radiation was used to determine phase analysis [4].

3. Results and discussion

The DNR produced by the casting process that show surface fracture (Fig. 1) were a hypoeutectic composition with various component alloys that contained Fe, C, Si, Mn, Ni, and other constituents, as shown in Table II. Several mechanisms occurred during solidification, such as the formation of phase, element solubility, and segregation, to name but a few. This alloyed iron consists of several phases, namely, austenite matrix, eutectic austenite, graphite aggregate, carbides, and inclusion of impurities. Ni and Si limit the solubility of graphite in austenite while Mn raises it. The following transformation is believed to occur during solidification [5]

$$\mathrm{L} \rightarrow \mathrm{L}_1\,\mathrm{L}_2 \rightarrow \mathrm{L}_1 + \gamma, \tag{1}$$

where L is liquid, L_1 and L_2 are liquid rich in positive and negative segregation elements, and γ is an austenite iron matrix. In general, the central section of the alloyed iron grain is rich in Ni and Si, while the outer section of grain, such as the last to freeze (LTF) region, is enriched with positive segregation elements, such as Mn [5]. The distribution of elements is shown in Table II. The X-ray diffraction analysis verified that the as-cast structures produced were a mixture of austenite and carbide, $Mn_{23}C_6$.

TABLE II

Elements constituent affected by micro segregation in the microstructure of alloyed irons [wt%]. A — Nodule graphite, B — Centre of dendrite area, C — Edge of dendrite area, D — LTF region.

	Position of electron probe			
	A	B	C	D
FeC (graphite)	100	0	0	0
Si	0	1.192	1.174	0.738
Ni	0	7.044	5643	4850
Mn	0	3.924	5.426	8.556
P	0	0	0	1.437

Specimen of 9Mn–10Ni wt% possesses not only the highest nodule count but oxide depth penetration as well. It was revealed that the alloyed iron with 9Mn–10Ni wt%, which acquires the least carbide, has suffered the most oxide depth penetration. Whereas, the alloyed iron with 12Mn–10Ni wt%, which acquires the most carbide composition,

TABLE III

Amounts of constituent in the microstructure and its mechanical properties of alloyed iron.

Material	γ-Fe	$Mn_{23}C_6$	Nodularity [%]	Nodule count [No/mm^2]	Elevated temperature ultimate tensile strength [MPa]
9Mn–10Ni	94.613	5.387	76.2	214	154 ± 7
10Mn–10Ni	93.963	6.037	73.3	203	150 ± 7
11Mn–10Ni	93.732	6.268	70.3	180	146 ± 7
12Mn–10Ni	93.651	6.349	67.4	174	143 ± 7

TABLE IV

Average oxide thickness in mm of specimen after 25 h furnace atmosphere–air (765°C) exposures.

Specimen (Mn [wt%])	Specimen thickness [mm]	Oxide depth [mm]			Total depth of attack [mm]	Percentage depth of attack [%]
		1st layer — outer	2nd layer —inner	3rd layer —inner		
12	15	0.1570	0.0991	0.0493	0.3054	2.04
11	15	0.1630	0.1250	0.0554	0.3434	2.29
10	15	0.1700	0.1170	0.0696	0.3566	2.38
9	15	0.1720	0.1350	0.0920	0.3990	2.66

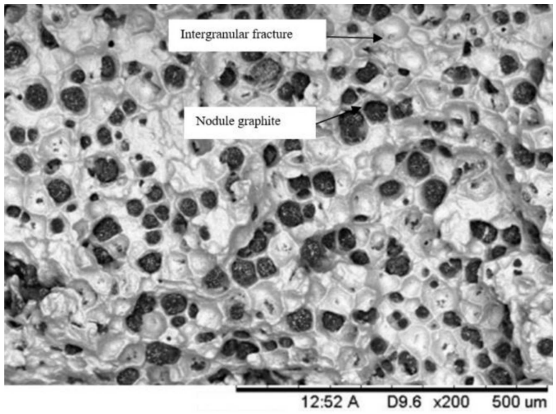

Fig. 1. SEM micrograph shows fracture surface of short term elevated tensile test. The entire surface experienced intergranular fracture.

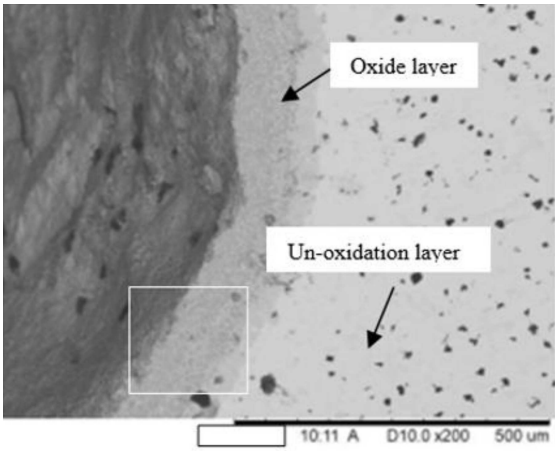

Fig. 2. SEM micrograph of the oxidized alloyed iron for 25 h in furnace atmosphere–air at 765°C.

has the least oxide depth penetration. It was noted that the alloyed iron with 9Mn–10Ni wt% has suffered the most oxide depth penetration. Whereas, alloyed iron with 12Mn–10Ni wt% has the least oxide depth penetration, as shown in Table III.

Figure 2 shows the surface and cross section morphologies of alloyed iron, oxidized in furnace atmosphere–air at 765°C for 25 h. The oxide surface was black and covered with whiskers with different thickness affected (Table IV). After 25 h, most of the outer Fe oxide layer spalled off upon cooling. It was composed of fine oxide precipitates embedded in a matrix containing Fe, Mn and Ni. The lack of Cr oxide is due to a lower Cr composition used during melting [6]. The outer oxide layer consisted of Fe oxides identified as awaruite, taenite, manganese-iron oxide, $MnFe_2O_4$, nickel iron oxide, and $NiFe_2O_4$. This outer oxide spalled off heavily in the form of large plates. Oxide spallation happened due to the stress generated by the growth of oxide during the oxidation period. The stress started to accumulate along with the oxide growth as weight was gained continuously. At a certain point, the scale thickness was unable to withstand the increasing stress, and thus released it. This release led to the cracking and spallation of oxide [7]. The inner oxide was composed of SiO_2, wustite, hematite, magnetite, iron manganese oxide, and austenite structure. Both inner oxide thicknesses indicated that a higher Mn [wt%] was less corroded and that the oxide thickness was lower. There is also the presence of SiO_2, which is known for its oxidation protective characteristics [8].

TABLE V

SEM EDS of oxidation elements [wt%] after 25 h furnace atmosphere–air (765°C) exposures.

Elements	Position of electron probe		
	1	2	3
oxygen	24.686	9.983	0
magnesium	0.015	0.056	0.141
silicon	4.149	3.626	2.925
chromium	0.161	0.236	0.264
manganese	5.722	6.536	9.473
nickel	7.074	6.745	5.617
iron	52.091	69.402	75.445

The oxidation mechanism is largely controlled by the diffusion rate of the reactive class through the scale [9]. The gradient concentration profiles observed at the interface of the metal–oxide indicate a slow diffusion process in the alloyed iron, as shown in Table IV.

Most probably, it occurred due to the compact austenite matrix of the alloyed iron. Therefore, the zone of inter-diffusion becomes narrow, and the metal–oxide interface is quite sharp. Most likely, as Fe ions migrated to the outer oxide boundary, the nobility of the Ni and Mn-rich bulk, together with oxygen solubility, was increased [9]. Possible reactions to the layers are as follows

$$M + 2O_2 \rightarrow MO_4(NiFe_2O_4), \quad (2)$$

$$M + 2O_2 \rightarrow MO_4(MnFe_2O_4), \quad (3)$$

$$M + O_2 \rightarrow MO_2(SiO_2). \quad (4)$$

Most of the graphite nodules restrained in and beneath the oxide layer were oxidized. Figure 2 also reveals trapped nodule graphite in the oxide layer that influenced cracking in the oxide layer. It occurred because oxygen was able to diffuse to the nodule graphite, leading to decarburization, as shown in Table V. Then, carbon easily reacted with oxygen before being decarburized. The crack in the oxide layer provided oxygen for a further diffusion path [10].

4. Conclusions

- Higher manganese addition has little significant effect on the elevated temperature tensile strength. Oxidation does weaken tensile properties due to the formation of altered phases at elevated temperatures. There is more carbide formed than free nodule graphite in the microstructure.
- A mixture of external oxide scale with the internal oxide of certain elements was formed in an alloyed iron (manganese, iron, and nickel oxide).
- Those layers occurred due to the precipitation of oxides within the alloyed iron matrix, which penetrated through the external scale in the alloy. Most probably, the activity of certain elements, such as the inward diffusion of oxygen, causes precipitation.

Acknowledgments

The authors would like to express their sincere thanks to Automotive Excellent Centre (AEC), Universiti Malaysia Pahang (UMP) and the Ministry of Higher Education (Malaysia) for providing laboratory facilities and financial assistance under project no. RDU190128@FRGS/1/2018/TK03/UMP/ 02/12.

References

[1] N. Fatahalla, A. AboElEzz, M.C. Semeida, *Mater. Sci. and Eng. A* **504,** 81 (2009).

[2] X. Jincheng, *Mater. and Design* **24**, 63 (2003).

[3] J.O. Choi, J.Y. Kim, C.O. Choi, J.K. Kim, P.K. Rohatgi, *Mater. Sci. and Eng. A* **383**, 323 (2004).

[4] L. Alvarez, C.J. Luis, I. Puertas, *J. Mater. Proc. Tech.* **153-154**, 1039 (2004).

[5] M.M. Rashidi, M.H. Idris, *Mater. Sci. and Eng. A* **574**, 226 (2013).

[6] M. Anderson, *Corr. Sci.* **53**, 10 (2011).

[7] J.H. Swisher, E.O. Fuchs, *Oxid. Metal.* **3**, 261 (1971).

[8] S.C. Tjong, *Mater. Char.* **30**, 4 (1993).

[9] F. Tholence, M. Norell, *Oxi. of Met.* **66**, 2 (2005).

[10] H. Ackermann, G. Teneva-Kosseva, K. Lucka, H. Koehne, S. Richter, J. Mayer, *Corr. Sci.* **49**, 3866 (2007).